J|A|C|S ARTICLES

Published on Web 12/24/2008

Iron Nanoparticle Growth in Organic Superstructures

Lise-Marie Lacroix,[†] Sébastien Lachaize,*[,†] Andrea Falqui,[†,§] Marc Respaud,[†] and Bruno Chaudret[‡]

Université de Toulouse, INSA, UPS, LPCNO, 135 avenue de Rangueil, F-31077 Toulouse, France, CNRS, LPCNO, F-31077 Toulouse, France, and Laboratoire de Chimie de Coordination du CNRS, 205 route de Narbonne, 31077 Toulouse Cedex 4, France

Received July 22, 2008; E-mail: sebastien.lachaize@insa-toulouse.fr

Abstract: A tunable synthesis of iron nanoparticles (NPs) based on the decomposition of $\{Fe[N(SiMe_3)_2]_2\}_2$ in the presence of organic superstructures composed of palmitic acid and hexadecylamine is reported. Control of the size (from 1.5 to 27 nm) and shape (spheres, cubes, or stars) of the NPs has been achieved. An environment-dependent growth model is proposed on the basis of results obtained for the NP morphology under various conditions and a complete Mössbauer study of the colloid composition at different reacting stages. It involves (i) an anisotropic growth process inside organic superstructures, leading to monocrystalline cubic NPs, and (ii) isotropic growth outside these superstructures, yielding polycrystalline spherical NPs.

Introduction

Many methods that are presently available for the synthesis of metal nanoparticles (NPs) lead to the formation of monodisperse objects.[1] These nano-objects can further self-organize when deposited on a surface or, in certain cases, directly form large superlattices in solution.[2] However, the processes leading to strict monodispersity of nanoparticles or to the formation of supercrystals in solution are not fully understood. Our group has obtained several metal nanoparticle superlattices composed of either tin, iron, or iron/cobalt.[3] We concentrate in this paper on the process of iron nanoparticle growth, given the present need for highly magnetic nanoparticles.

Magnetic nanoparticles are attractive for various applications provided that strong control of their physical properties can be achieved.[4,5] Metallic iron has a high magnetization at room temperature [M_S(bulk) = 212 emu g^{-1}] and a superparamagnetic behavior (for sizes ranging from 1 to 12 nm) that, from a physical point of view, makes it a material of choice for biomedical applications such as magnetic fluid hyperthermia (MFH) and magnetic resonance imaging (MRI).[6] However, its high reactivity, especially with dioxygen, makes it unusable under these conditions if unprotected. Our research aims at producing magnetic core/shell nanoparticles that take advantage of an iron core whose magnetic properties are preserved from degradation by means of a protective layer.[7] Before taking up this challenge, we first worked on the adjustment of the magnetic properties of the iron core for the above-mentioned applications, that is to say, the adjustment of its size and shape and the nature of surface ligands. Therefore, a good understanding of iron NP formation is a crucial point.[1a,8] Several research groups have already prepared iron NPs of very good quality, but usually with magnetizations lower than that of the bulk, especially at small sizes.[2a,9] In addition, some knowledge has already been reported on size control in different studies: in particular, it has been pointed out that the acid concentration is a key parameter.[9f,10] Our group has previously reported that the reduction of $\{Fe[N(SiMe_3)_2]_2\}_2$ under H_2 leads to unoxidized, small iron NPs of homogeneous size near 1.5 nm that exhibit bulk magnetization.[11] The same method leads to larger and well-defined NPs with bulk magnetization when a mixture of long-chain acid and

[†] Université de Toulouse and LPCNO.
[‡] Laboratoire de Chimie de Coordination du CNRS.
[§] Present address: Fondazione Istituto Italiano di Tecnologia (IIT), Via Morego 30, 16163 Genova, Italy.

(1) (a) Yin, Y.; Alivisatos, A. P. *Nature* **2005**, *437*, 664–670. (b) Park, J.; Joo, J.; Kwon, S. G.; Jang, Y.; Hyeon, T. *Angew. Chem., Int. Ed.* **2007**, *46*, 4630–4660. (c) Hyeon, T. *Chem. Commun.* **2003**, *927*, 934.
(2) (a) Sun, S.; Zeng, H. *J. Am. Chem. Soc.* **2002**, *124*, 8204–8205. (b) Park, J.; An, K.; Hwang, Y.; Park, J. G.; Noh, H. J.; Kim, J. Y.; Park, J. H.; Hwang, N. M.; Hyeon, T. *Nat. Mater.* **2004**, *3*, 891–895. (c) Sun, S.; Murray, C. B. *J. Appl. Phys.* **1999**, *85*, 4325–4330. (d) Soulantica, K.; Maisonnat, A.; Senocq, F.; Fromen, M.-C.; Casanove, M.-J.; Chaudret, B. *Angew. Chem., Int. Ed.* **2001**, *40*, 2984–2986. (e) Legrand, J.; Ngo, A.-T.; Petit, C.; Pileni, M.-P. *Adv. Mater.* **2001**, *13*, 58–61.
(3) (a) Dumestre, F.; Chaudret, B.; Amiens, C.; Renaud, P.; Fejes, P. *Science* **2004**, *303*, 821–823. (b) Soulantica, K.; Maisonnat, A.; Fromen, M.-C.; Casanove, M.-J.; Chaudret, B. *Angew. Chem., Int. Ed.* **2003**, *42*, 1945–1949. (c) Desvaux, C.; Amiens, C.; Fejes, P.; Renaud, P.; Respaud, M.; Lecante, P.; Snoeck, E.; Chaudret, B. *Nat. Mater.* **2005**, *4*, 750–753.
(4) (a) Sun, S.; Murray, C. B.; Weller, D.; Folks, L.; Moser, A. *Science* **2000**, *287*, 1989–1992. (b) Toneguzzo, P.; Viau, G.; Acher, O.; Fiévet-Vincent, F.; Fiévet, F. *Adv. Mater.* **1998**, *10*, 1032–1035. (c) Maurer, T.; Ott, F.; Chaboussant, G.; Soumare, Y.; Piquemal, J.-Y.; Viau, G. *Appl. Phys. Lett.* **2007**, *91*, 17501. (d) Jeong, U.; Teng, X.; Wang, Y.; Yang, H.; Xia, Y. *Adv. Mater.* **2007**, *19*, 33–60. (e) Ito, A.; Shinkai, M.; Honda, H.; Kobayashi, T. *J. Biosci. Bioeng.* **2005**, *100*, 1–11.
(5) (a) Lu, A.-H.; Salabas, E. L.; Schüth, F. *Angew. Chem., Int. Ed.* **2007**, *46*, 1222–1244. (b) Capek, I. *Adv. Colloid Interface Sci.* **2004**, *110*, 49–74. (c) Suslick, S. K.; Fang, M.; Hyeon, T. *J. Am. Chem. Soc.* **1996**, *118*, 11960–11961.
(6) (a) Hergt, R.; Dutz, S.; Müller, R.; Zeisberger, M. *J. Phys.: Condens. Matter* **2006**, *18*, S2919–S2934. (b) Habib, A. H.; Ondeck, C. L.; Chaudhary, P.; Bockstaller, M. R.; McHenry, M. E. *J. Appl. Phys.* **2008**, *103*, 07A307. (c) Bautista, M. C.; Bomati-Miguel, O.; Zhao, X.; Morales, M. P.; Gonzalez-Carreno, T.; de Alejo, R. P.; Ruiz-Cabello, J.; Veintemillas-Verdaguer, S. *Nanotechnology* **2004**, *15*, S154–S159. (d) Cho, S. J.; Jarrett, B. R.; Louie, A. Y.; Kauzlarich, S. M. *Nanotechnology* **2006**, *17*, 640–644.
(7) Salgueiriño-Maceira, V.; Correa-Duarte, M. A. *Adv. Mater.* **2007**, *19*, 4131–4144.

amine is added. Using the amido precursor $Fe[N(SiMe_3)_2]_2(THF)$ (Me = CH_3, THF = tetrahydrofuran) in the presence of oleic acid and hexadecylamine (HDA), Dumestre et al.[3a] have prepared 7 nm iron nanocubes organized into superlattices. The growth process and control of size (in this case limited to 7 nm) and shape (spherical, cubic or anisotropic) were not achieved on this system, however. We have therefore extended the study in order to understand and possibly propose a model for the size and shape control of iron NPs prepared in the presence of such surfactant mixtures. The route we have chosen is the decomposition of $\{Fe[N(SiMe_3)_2]_2\}_2$ in the presence of HDA and palmitic acid (PA) under mild conditions. Several experimental parameters have been examined and tuned with the aim of understanding their influence on the mean size and shape of the final NPs in order to produce high-quality colloidal samples that could cover the superparamagnetic range of interest. Supported by a complete Mössbauer study of the colloid composition at different reacting stages, this work has lead to the proposition of an environment-dependent growth mechanism.

Materials and Methods

General Procedures. Mesitylene (Fluka, ≥99%) was distilled over sodium according to standard procedures. PA (Sigma, ≥99%) and HDA (Fluka, ≥99%) were used without any additional purification. Reactants and products were stored and manipulated in an argon glovebox exclusively. The reactants were mixed together at room temperature, and all of the syntheses were performed in Fischer−Porter bottles.

NPs were obtained by decomposition of the iron dimer $\{Fe[N(SiMe_3)_2]_2\}_2$.[12] Both kinds of reactions were performed in the presence of HDA and PA in mesitylene under a reductive atmosphere of dihydrogen (3 bar). The general conditions were adjusted to study the reaction kinetics (reaction time varying from 30 min to 48 h), the influence of temperature (from 100 to 150 °C), and surfactant concentration effects.

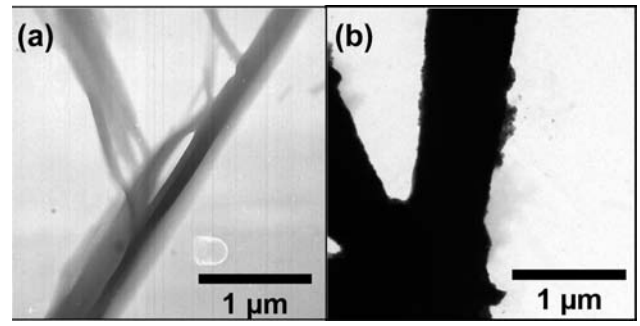

Figure 1. TEM pictures of micrometric superstructures observed (a) prior to reaction under H_2 and (b) after 48 h of reaction.

Synthesis of Nanocube Superlattices. A colorless solution of PA (384 mg, 1.5 mmol, 1.5 equiv per mol of iron) in mesitylene (10 mL) was added to a green solution of $\{Fe[N(SiMe_3)_2]_2\}_2$ (376 mg, 0.5 mmol) in mesitylene (5 mL). The mixture was manually stirred, and its color immediately changed to yellow. After 1 min, a solution of HDA (482 mg, 2.0 mmol, 2.0 equiv) in mesitylene (5 mL) was added to it. The mixture started to darken and became black after 10 min of magnetic stirring at room temperature. The solution was then put under 3 bar of H_2 and allowed to react in an oil bath at 150 °C for 48 h.

The monitoring of this reaction was performed on the same sample equally distributed into five Fisher−Porter bottles, each of which was placed in the same oil bath (150 °C) for a specified time (0.5, 2, 6, 12, or 25 h).

Characterization of the NPs. Microscopy samples were prepared by deposition of a drop of diluted colloidal solution onto a carbon-coated copper grid and observed on a JEOL 6700F microscope for scanning electronic microscopy (SEM), a JEOL 1011 microscope for bright-field transmission electronic microscopy (TEM), or a JEOL-2100F field-emission microscope for high-resolution TEM (HRTEM), the latter two working at 100 and 200 kV, respectively. In the majority of cases, size histograms were obtained by an automatic counting process over 500 particles;[13] on particular samples (stars and large cubes), counting was done manually for at least 100 nanoparticles. Size distributions were fitted by the Gaussian law; the results are expressed in terms of the calculated mean size and the standard deviation (σ). Magnetic studies were carried out on powder samples by SQuID (Quantum Design MPMS 5.5), and the iron state and environment were analyzed by Mössbauer spectroscopy (WISSEL, ^{57}Co source). Samples were prepared in the glovebox, and extreme care was taken to avoid oxidation during transfer to the apparatus. Flame-sealed glass tubes of powder were prepared under argon to determine the iron composition from microanalysis measurements performed by inductively coupled plasma (ICP).

Results

On the basis of the results obtained by Dumestre et al.,[3a] we used a combination of PA and HDA to grow well-defined NPs. We successively monitored the kinetics of the reaction, the influence of the temperature, and finally the influence of the acid/amine ratio, as presented hereafter. The first observation that actually started this study was made before any NPs were formed: a mixture of PA/HDA in a 1.5:2 ratio mixed with $\{Fe[N(SiMe_3)_2]_2\}_2$ at room temperature led immediately to the formation of organic superstructures in mesitylene, as revealed by TEM (see Figure 1a). Size measurements by dynamic light scattering from the starting solution (after heating at only 50 °C for 10 min) also confirmed the formation of micrometric

(8) (a) Finney, E. E.; Finke, R. G. *J. Colloid Interface Sci.* **2008**, *317*, 351–374. (b) Dumestre, F.; Chaudret, B.; Amiens, C.; Fromen, M.-C.; Casanove, M.-J.; Renaud, P.; Zurcher, P. *Angew. Chem., Int. Ed.* **2002**, *41*, 4286–4289. (c) Puntes, V. F.; Zanchet, D.; Erdonnez, C. K.; Alivisatos, A. P. *J. Am. Chem. Soc.* **2002**, *124*, 12874–12880. (d) Shevchenko, E. V.; Talapin, D. V.; Schnablegger, H.; Kornowski, A.; Festin, Ö.; Svedlindh, P.; Haase, M.; Weller, H. *J. Am. Chem. Soc.* **2003**, *125*, 9090–9101. (e) Ung, D.; Soumare, Y.; Chakroune, N.; Viau, G.; Vaulay, M.-J.; Richard, V.; Fiévet, F. *Chem. Mater.* **2007**, *19*, 2084–2094. (f) Pei, W.; Kakibe, S.; Ohta, I.; Takahashi, M. *IEEE Trans. Magn.* **2005**, *41*, 3391–3393. (g) Liang, X.; Wang, X.; Zhunang, J.; Chen, Y.; Wang, D.; Li, Y. *Adv. Funct. Mater.* **2006**, *16*, 1805–1813. (h) Casula, M. F.; Jun, Y.-W.; Zaziski, D. J.; Chan, E. M.; Corrias, A.; Alivisatos, A. P. *J. Am. Chem. Soc.* **2006**, *128*, 12675–1682.

(9) (a) Huber, D. L. *Small* **2005**, *1*, 482–501. (b) Huber, D. L.; Venturini, E. L.; Martin, J. E.; Provencio, P. P.; Patel, R. J. *J. Magn. Magn. Mater.* **2004**, *278*, 311–316. (c) Sun, S.; Zeng, H.; Robinson, D. B.; Raoux, S.; Rice, P. M.; Wang, S. X.; Li, G. *J. Am. Chem. Soc.* **2004**, *126*, 273–279. (d) Peng, S.; Wang, C.; Xie, J.; Sun, S. *J. Am. Chem. Soc.* **2006**, *128*, 10676–10677. (e) Farrell, D.; Majetich, S. A.; Wilcoxon, J. P. *J. Phys. Chem. B* **2003**, *107*, 11022–11030. (f) Farrell, D.; Cheng, Y.; McCallum, R. W.; Sachan, M.; Majetich, S. A. *J. Phys. Chem. B* **2005**, *109*, 13409–13419. (g) Hyeon, T.; Lee, S. S.; Park, J.; Chung, Y.; Na, H. B. *J. Am. Chem. Soc.* **2001**, *123*, 12798–12801. (h) Kim, D.; Park, J.; An, K.; Yang, N.; Park, J.; Hyeon, T. *J. Am. Chem. Soc.* **2007**, *129*, 5812–5813. (i) Yang, H. T.; Ogawa, T.; Hasegawa, D.; Takahashi, M. *Phys. Status Solidi A* **2007**, *204*, 4013–4016. (j) Shavel, A.; Rodriguez-Gonzales, B.; Spasova, M.; Farle, M.; Liz-Marzan, L. M. *Adv. Funct. Mater.* **2007**, *17*, 3870–3876.

(10) Yang, H.; Ito, F.; Hasegawa, D.; Ogawa, T.; Takahashi, M. *J. Appl. Phys.* **2007**, *101*, 09J112.

(11) Lacroix, L.-M.; Lachaize, S.; Falqui, A.; Blon, T.; Carrey, J.; Respaud, M.; Dumestre, F.; Amiens, C.; Margeat, O.; Chaudret, B.; Lecante, P.; Snoeck, E. *J. Appl. Phys.* **2008**, *103*, 07D521.

(12) Olmstead, M. M.; Power, P. P.; Shoner, S. C. *Inorg. Chem.* **1991**, *30*, 2547–2551.

(13) Rasband, W. S. *ImageJ*; National Institutes of Health: Bethesda, MD, 1997−2007; http://rsb.info.nih.gov/ij/ (accessed Dec 4, 2008).

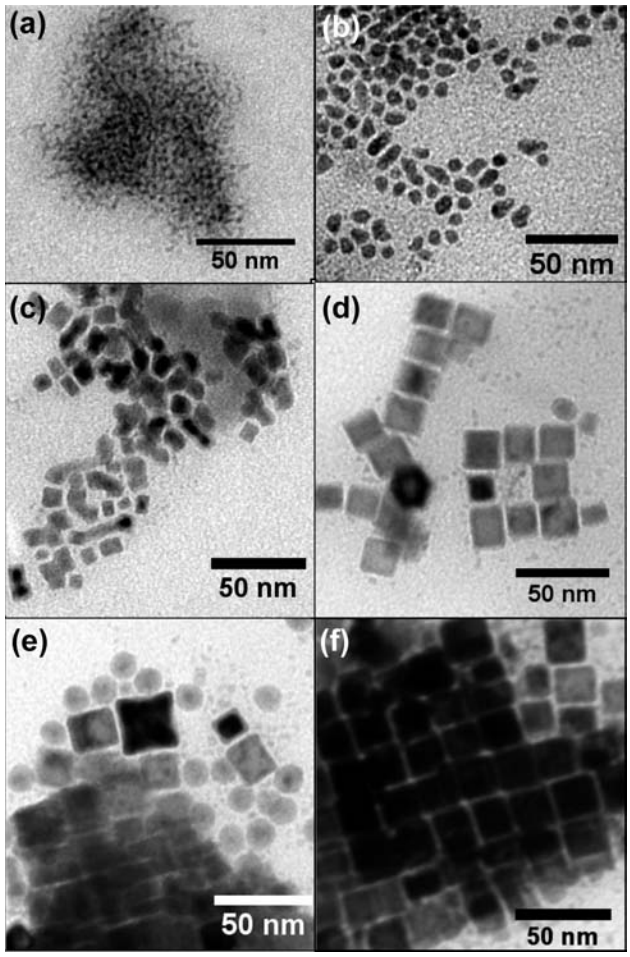

Figure 2. TEM pictures of nanoparticles stabilized by a 1.5:2 PA/HDA mixture after (a) 0.5, (b) 2, (c) 6, (d) 12, (e) 25, and (f) 48 h of reaction.

objects (see Figure S1 in the Supporting Information). The nature of the surfactants and the observed shape of these micrometric stable objects are in good agreement with the formation of a mesophase with a lamellar structure.[14,15] Moreover, the TEM picture's contrast on these structures indicates the presence of iron, which is certainly involved in molecular species and/or clusters. The formation of these iron-filled organic superstructures is correlated with the appearance of similar superstructures containing nanocubes observed after heating of the same solution under dihydrogen for 48 h (see Figure 1b), as shown in this article.

Kinetics of NP Growth. In order to understand the correlation between the superstructures observed at $t = 0$ and $t = 48$ h, the kinetics of the iron dimer decomposition in the presence of 1.5:2 PA/HDA has been monitored. We particularly focused on what happened inside the organic superstructures, and therefore, the TEM pictures in Figure 2 show only these regions (a larger view of each region of interest is available in Figures S2, S3, and S4 in the Supporting Information). After 30 min at 150 °C under dihydrogen, very small (<2 nm) NPs that we will call

(14) Dubois, M.; Lizunov, V.; Meister, A.; Gulik-Krzywicki, T.; Verbavatz, J. M.; Perez, E.; Zimmerberg, J.; Zemb, T. *Proc. Natl. Acad. Sci. U.S.A.* **2004**, *101*, 15082–15087.

(15) (a) Karlsson, S.; Friman, R.; Lindstrom, B.; Backlund, S. *J. Colloid Interface Sci.* **2001**, *243*, 241–247. (b) Abécassis, B.; Testard, F.; Arleth, L.; Hansen, S.; Grillo, I.; Zemb, T. *Langmuir* **2006**, *22*, 8017–8028.

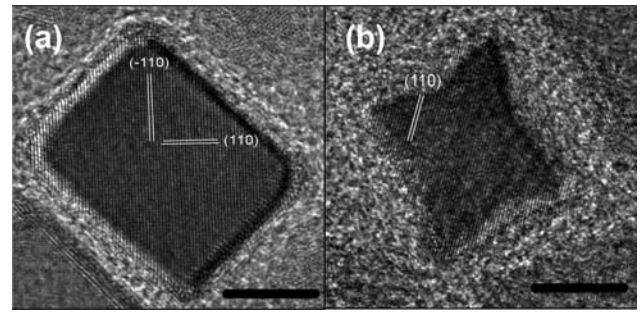

Figure 3. HRTEM pictures of monocrystalline octapods and cubic NPs. The {110} planes of the iron bcc crystal structure are highlighted. The scale bar represents 5 nm.

"nuclei" are formed (see Figure 2a). After 2 h, we observed ~5 nm spherical NPs and anisotropic NPs displaying a width of ~5 nm and a length of ~10 nm (see Figure 2b). A majority of the nuclei were still detected around these misshapen NPs. Some were still present even after 6 h, but by this time the sample was predominantly composed of larger NPs (see Figure 2c and Figures S2c and S3 in the Supporting Information). Most of these anisotropic NPs had at least one dimension between 25 and 50 nm (32.6 nm, $\sigma = 7.4$ nm), and some well-defined facets became apparent. A few cubic NPs displaying round edges (11.0 nm, $\sigma = 1.0$ nm) were also observed. The anisotropic particles observed at this stage of the reaction result from coalescence. They disappeared with time while particles of cubic shape were formed. As a matter of fact, after 12 h, the cubic NPs became predominant (17.0 nm, $\sigma = 1.7$ nm; see Figure 2d). After 25 h, large superlattices with lengths of several microns, containing mainly cubic NPs (20.7 nm, $\sigma = 0.9$ nm) but also some not completely filled octapods, were observed. These objects were on their way to form cubes, indicating that the reaction, though at a very advanced stage, was not yet complete (see Figure 2e and Figures S2e and S4 in the Supporting Information). The spherical NPs observed around the nanocube superlattice (NCS) at this point look well-defined, with a mean diameter of 13.2 nm ($\sigma = 1.2$ nm). Finally, after 48 h of reaction, NCSs composed of cubic NPs (20.9 nm, $\sigma = 2.7$ nm; see Figures 2f and 1b) were obtained, together with a few spherical NPs outside them (12.0 nm, $\sigma = 1.0$ nm; see the inset of Figure S2f in the Supporting Information). The system did not change much after 7 days at 150 °C. Consequently, 48 h of reaction was kept as a reference for the other experiments performed at 150 °C.

The crystal structures of the different iron NPs obtained above were investigated by HRTEM (see Figure 3). The octapods and cubic NPs are monocrystalline and exhibit a bcc structure; the cubic NPs expose only {100} planes at their surface, while the octapods also expose {110} planes. Because of air exposure during the transfer of the carbon grid to the microscope chamber, the observed NPs are partially oxidized. The spherical NPs observed outside the organic superstructures are polycrystalline (see Figure S5 in the Supporting Information).

To gain some information on the rate law of this growth process, and especially to shed light on the evolution of the balance between Fe(II) and Fe(0) species, systematic Mössbauer spectroscopy and magnetization measurements were carried out on the raw material at different reaction stages. Figure 4 displays the Mössbauer spectra at $t = 0$, 2, 6, 12, and 48 h, and Table 1 summarizes the fit parameters (also see Table S1 and Figures S6, S7, and S8 in the Supporting Information for additional details about the Mössbauer and SQuID experiments). As a

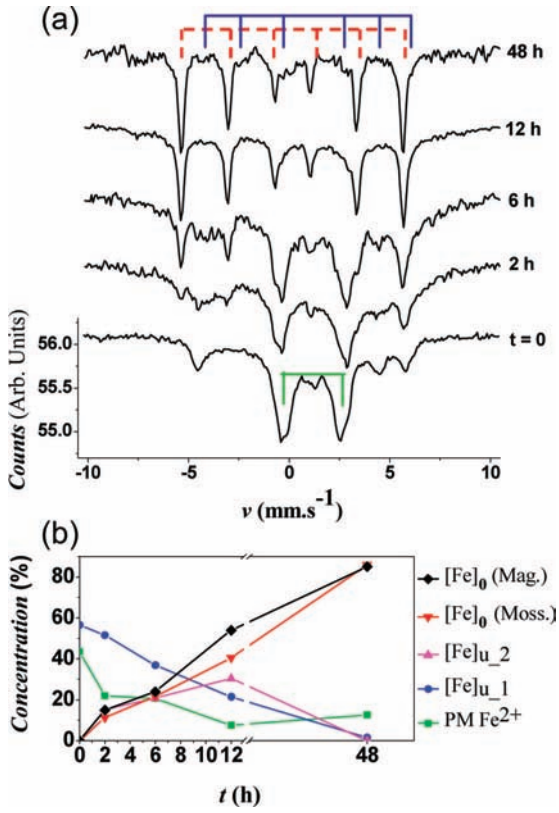

Figure 4. (a) Mössbauer spectra of the PA/HDA/iron system at different stages of the reaction. (b) Evolution of the species concentrations as a function of the reaction time, as deduced from fits of the Mössbauer spectra.

Table 1. Contribution Parameters Used to Fit the Mössbauer Spectra[a]

		contribution at time *t*				
species	parameter(s)	0	2 h	6 h	12 h	48 h
PM Fe^{2+}	$\delta = 1.16$, $Q = 2.5$	18.7%	3.7%	2.5%	0.9%	−
	$\delta = 1.2$, $Q = 3.15$	16.1%	12.9%	14.5%	0.9%	7.7%
	$\delta = 1.16$, $Q = 3.65$	8.7%	5.3%	3.7%	5.7%	4.9%
	$<Q>$	2.97	3.16	3.16	3.45	3.34
$[Fe]_{u\_1}$	δ	1.14	1.21	1.16	1.14	−
	Q	−0.95	−0.95	−0.75	−0.7	−
	H_{hyp}[b]	−	249	245	202	−
$[Fe]_{u\_2}$	δ	−		0.45		−
	Q	−		0		−
	H_{hyp}	−		400−450		−
$[Fe]_0$	δ	−	0.15	0.1	0.1	0.1
	Q	−	0	0	0	0
	H_{hyp}	−		330−340		

[a] Units: δ and Q are given in mm s^{-1}, and H_{hyp} is given in kG. [b] The mean value is given in this case.

general feature, one can notice the gradual change of the absorption up to a sextet consisting of ferromagnetic α-Fe after 48 h of reaction. Even prior to reaction with H_2 ($t = 0$), the single doublet of the $\{Fe[N(SiMe_3)_2]_2\}_2$ precursor does not contribute to the spectrum; thus, the precursor quantitatively reacts with the PA/HDA mixture. Adding either PA or HDA to $\{Fe[N(SiMe_3)_2]_2\}_2$ in a 2:1 ligand-to-iron ratio leads to new species of a different nature (Figures S9 and S10 in the Supporting Information display the corresponding spectra and the magnetization curves, respectively). In the case of only HDA, the Mössbauer spectrum evidences a well-defined sextet and the hysteresis curve displays a characteristic weak magnetization with high-field irreversibility. This material behaves as a well-compensated antiferromagnet. On the contrary, the Mössbauer spectrum evidences a wide doublet in the case of PA: the main contribution is characteristic of molecular iron(II) species, while the small one arises from coupled iron(II) cations. This material has a rather high magnetization and a weak hysteresis curve.

Eventually, reaction of the $\{Fe[N(SiMe_3)_2]_2\}_2$ precursor with a 1.5:2 PA/HDA mixture leads to a material with an intermediate spectrum. A wide doublet similar to the one measured in the case of PA again indicates the presence of a paramagnetic iron(II) carboxylate material, denoted as PM Fe^{2+}. A second and much more complex contribution, denoted $[Fe]_{u\_1}$, is characterized by a broad distribution of hyperfine fields (H_{hyp}), a large isomer shift (δ) in the same range as for the PM Fe^{2+} species, and a quite large negative quadrupolar effect (Q). The measured magnetic moment per Fe atom is weak but still higher than in the case of pure amine system. Although the identification of this material deserves much more work, Mössbauer spectroscopy reveals iron(II) cations in a complex chemical environment that combines carboxylate and amine ligands. We assume this material to mainly compose the large organic superstructures observed by TEM (see Figure 1a), and we will now call it the iron(II) reservoir.

The consumption of the iron(II) reservoir is quite slow; its fingerprint is indeed still observed after 12 h of reaction. Its decrease is accompanied by an increase of an Fe(0) contribution (denoted $[Fe]_0$). An intermediate phase (denoted $[Fe]_{u\_2}$) with large hyperfine contributions of up to 45 T grows in during the first hours of reaction before being totally consumed at the end. After 2 h, the Fe(0) nuclei clearly observed by TEM (see Figure 2b) contribute only 13% of the total spectrum. After 6 h, their contribution increases slightly to 22%, with the iron(II) reservoir still being the majority. After 12 h, the balance is modified in favor of $[Fe]_0$, which at this time represents 53%. It increases to 85.9% after 48 h, while the iron(II) reservoir remains only as a small part of the carboxylate iron(II) contribution (14.1%) which is probably due to the equilibrium between Fe^0 and Fe^{2+} under these particular conditions (the presence of H_2 and acid) and to the surface coordination of carboxylate groups oxidatively added on the surface of the particles. We also report the evolution of the spontaneous magnetization deduced from the low-temperature magnetic measurements by SQuID (labeled "$[Fe]_0$ (Mag.)" in Figure 4b). It agrees well with the one deduced from the Mössbauer spectra.

The kinetic study of the reaction, followed by TEM and Mössbauer spectroscopy, evidence a series of complex reaction steps leading to the formation of the iron NCSs. The Mössbauer study shows that the iron(0) NPs are obtained through numerous intermediate phases that slowly feed the growth; their exact identification will require some more work to be done. We assume that at least one of them concerns Fe(II) cations entrapped in the organic superstructures observed by TEM. Thus, in regard to these results, it is possible to decompose the growth inside these organic superstructures into three main steps: (i) nucleation, (ii) isotropic growth and coalescence, which first lead to some anisotropic NPs, and finally (iii) oriented growth and repair mechanisms to form in the end mainly cubic NPs organized into superlattices. Each of these processes is characterized by a different energy barrier. In order to gain some knowledge about these activation energies, various syntheses were performed with the 1.5:2 PA/HDA system at different temperatures.

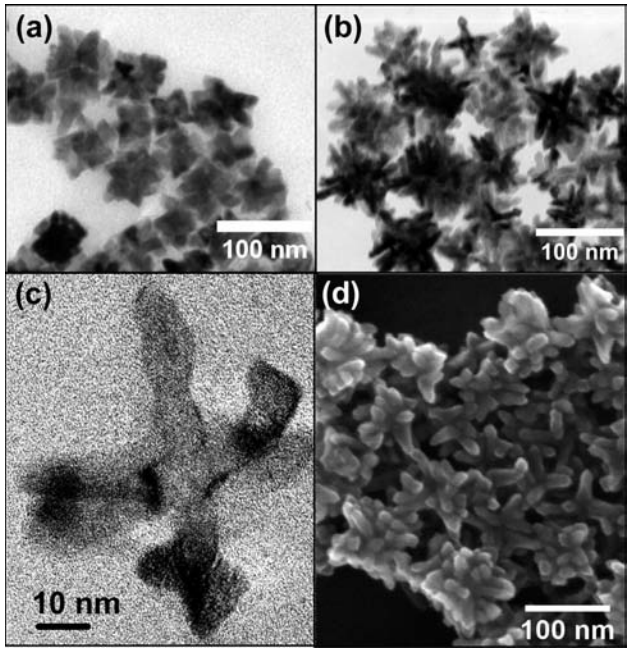

Figure 5. TEM pictures of nanoparticles obtained with a 1.5:2 ratio of PA/HDA (a) at 135 °C after 7 days and (b) at 120 °C after 21 days. (c) HRTEM picture of a starlike-shaped NP formed at 120 °C. (d) SEM picture of an aggregate of starlike-shaped NPs.

Influence of Temperature on NP Growth. We followed the reactions for 2, 7, 21, and 28 days at three different temperatures: 135, 120, and 100 °C. Since the temperature decrease leads to slower reactions, we adjusted the reaction times to reach the same reaction advancement. At 135 °C, after 7 days we ended up with large objects (46 nm, $\sigma = 4$ nm) clearly composed of several coalesced but faceted NPs (18.6 nm, $\sigma = 3.1$ nm) (see Figure 5a). They were stable over 21 days of reaction. Cubic NPs were not observed under these conditions. This result was not just a consequence of the longer reaction time, since as already mentioned above, the NCSs heated to 150 °C for 7 days did not change at all. At 120 °C, we observed the formation of anisotropic particles with starlike shapes after 21 days (see Figure 5b−d). Most of these stars expose six legs, but NPs with fewer branches were also observed (see Figures S11, S12, and S13 in the Supporting Information). Foot-type defects are present at the extremities of some legs (see Figure 5c). These "feet" are triangular and expose both {100} and {110} planes on their surfaces. A mean leg length of 30 nm was estimated from isolated stars. At 100 °C, comparable NPs were produced after 21 days of reaction, but the colloidal solution obtained in this case appeared to be very inhomogeneous, with either small NPs or stars (with leg lengths of ∼60 nm). These anisotropic particles may result from the growth of coalesced NPs similar to those formed after 6 h at 150 °C. Since the temperature decrease may affect each reaction step differently, one can consider that the coalescence step (ii) is maintained but the rate of the repair mechanism step (iii) is drastically reduced. As a consequence, anisotropic NPs are stabilized at temperatures lower than 150 °C.

Influence of Acid Concentration on Size and Shape. To verify the idea of a strong correlation between the initially formed organic superstructures and the NCS, we have looked at a reaction in which the former should not be formed: no organic superstructure was detected in the absence of carboxylic acid, for example. In this case, a 48 h reaction yielded wormlike NPs

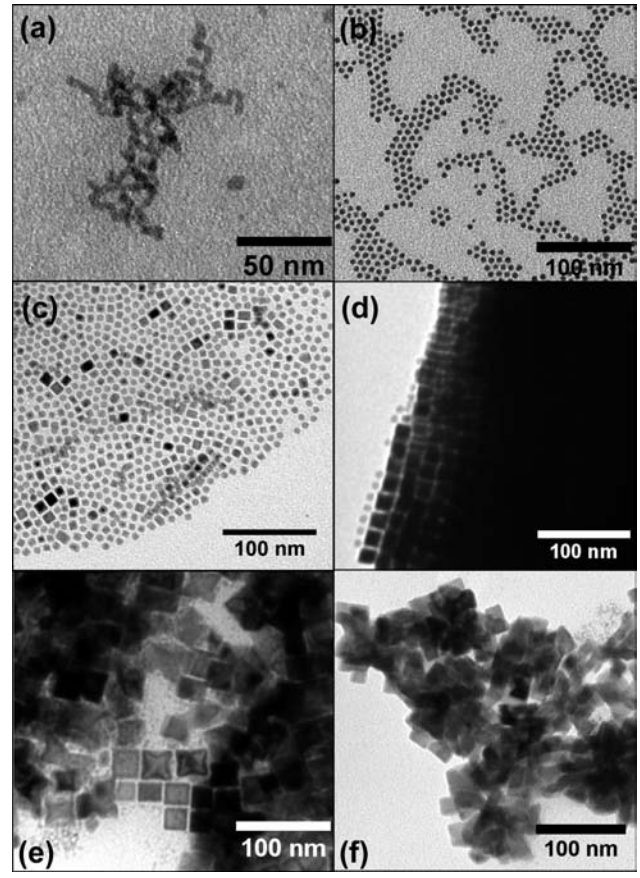

Figure 6. TEM pictures of NPs obtained by decomposition at 150 °C for 48 h in the presence of 2 equiv of HDA but different acid concentrations: (a) 0, (b) 1, (c) 1.2, (d) 1.4, (e) 1.6, and (f) 1.8 equiv.

only (see Figure 6a). In order to gain some understanding of the role of the acid, we investigated different acid concentrations. For this purpose, we kept the amine concentration constant at 2 equiv with respect to the iron molarity and varied the acid concentration from 1 to 1.8 equiv (the temperature and reaction time were again 150 °C and 48 h, respectively). Table 2 and Figure 6 sum up the experimental conditions and the results for each reaction (see also Figures S14 and S17 in the Supporting Information). At 1 equiv of PA (reaction A), we detected only spherical NPs with a narrow size distribution centered at 5.4 nm ($\sigma = 0.5$ nm). These NPs tended to self-organize on the TEM grid because of their narrow size distribution, but no traces of any 3D superstructures were found. Although the NPs were mostly spherical at 1.2 equiv of PA (reaction B), some cubic NPs appeared, generally surrounded by other faceted or spherical NPs inside quite large organizations. At 1.4 equiv of PA (reaction C), most of the NPs were cubic (13.3 nm, $\sigma = 1.0$ nm) and self-organized into micrometric superlattices. A few spherical NPs were present outside these structures. Furthermore, two size populations were found for them: the minor one was centered at 2.2 nm ($\sigma = 0.5$ nm) and the major one at 7.6 nm ($\sigma = 0.7$ nm). At 1.6 equiv of PA (reaction D), a colloidal solution composed of nuclei, octapods, and polydispersed cubic NPs (27.9 nm, $\sigma = 7.0$ nm) was obtained. The contrast on the TEM picture indicates that they were all entrapped in an amorphous medium, probably an organic shell containing some molecular iron. Finally, at 1.8 equiv (reaction E), the solution was composed of nuclei and large coalesced, faceted NPs (>50 nm). These coalesced NPs were very similar to the ones obtained at 135 °C for a PA/

Table 2. Reaction Summary

	A	B	C	reference	D	E	ref 3a
amine/acid ratio	2:1	2:1.2	2:1.4	2:1.5	2:1.6	2:1.8	2.38:1.19
NP type[a] (average size[b])	spheres (5.4)	spheres (6.9) cubes (13.3)	cubes (13.0) spheres (8.9)	cubes (20.9) spheres (12.0)	cubes (27.0) filled octapods spheres	coalesced faceted	cubes (7.0)

[a] The major type, as estimated on the basis of TEM pictures, is cited first. [b] Average sizes are given in nm.

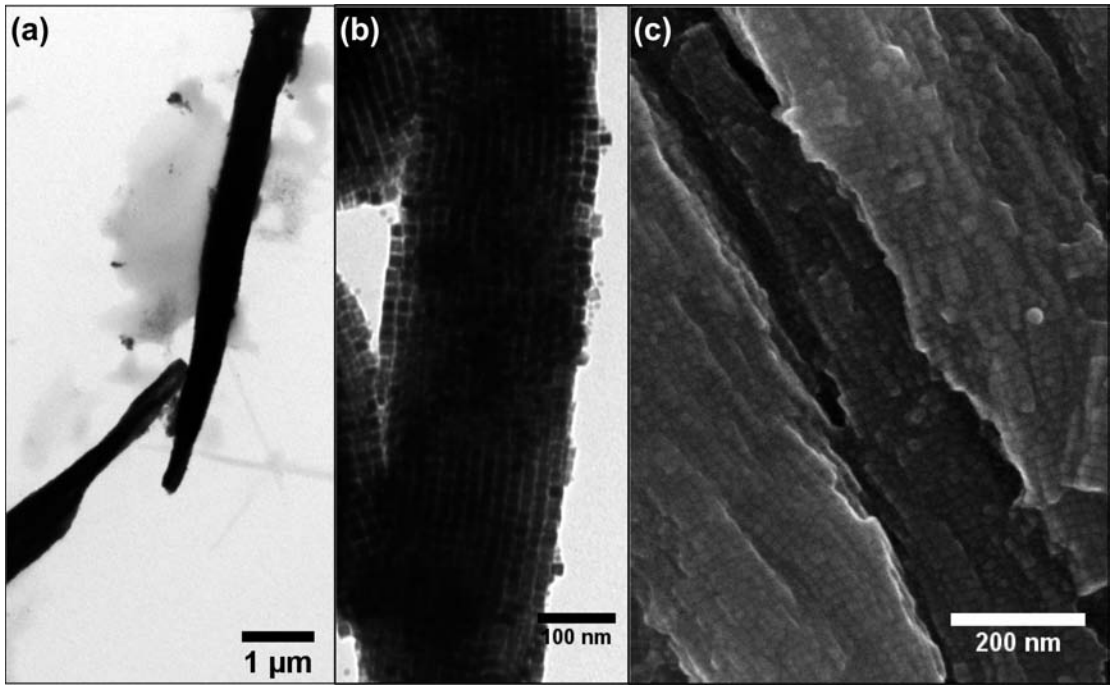

Figure 7. Micrometric iron nanocube superlattices formed in reaction C and observed by (a, b) TEM and (c) SEM. The 13.3 nm nanocubes are monodispersed ($\sigma = 1.0$ nm).

HDA ratio of 1.5:2 (see Figure 5a). Though they were quite large, both of them seemed to be grown under conditions similar to those for the NPs detected after 6 h in the reference reaction (see Figure 2c). Again, these NPs were located inside an amorphous medium.

From 1.4 to 1.8 equiv of PA, the NPs were enclosed in an organic superstructure constituted of HDA and PA. However, it was only for 1.4 and 1.5 equiv of PA (at 150 °C) that micrometric superlattices were detected. They were composed of closely packed monodispersed cubic NPs (13.3 and 20.3 nm, respectively), as revealed by TEM and SEM (see Figure 7). Upon comparison of these two cases, it seems that the smaller the nanocubes are, the larger are the superlattices. This might be correlated to the size distribution getting larger when the mean size increases, indicating that the long-range organization is less favored. The NCSs correspond to extended 3D superstructures formed in solution and not to self-assemblies driven by solvent evaporation. As previously explained by Dumestre et al.,[3a] they can be seen as the result of the concomitant crystallization of the nanoparticles and their ligand shells. This study actually has uncovered new evidence to aid in understanding the mechanism of their formation in solution. In fact, it is more correct to speak about the growth and shaping of cubic NPs inside a preformed organic superstructure, as discussed below.

Discussion

The results described above regarding the formation of iron NPs in the presence of PA and HDA suggest that the formation of spherical or cubic NPs depends on the growth environment. Formation of cubes for an acid/amine ratio of 1.4:2 or 1.5:2 is indeed associated with the presence of micrometric superlattices. It can be then inferred that growth of cubic NPs is strongly correlated with the organic superstructures preformed in solution while growth of spherical NPs occurs independently.

On the basis of this observation, the environment-dependent growth mechanism schematically represented in Figure 8 is proposed. This model takes into account the influence of the local acid concentration on every step of the NP synthesis and especially on their faceting. In particular, the model stems from the observations made during the kinetic study of our reference reaction (PA/HDA ratio of 1.5:2), which evidenced the presence of (i) nucleation, (ii) isotropic growth and coalescence, and (iii) oriented growth and repair mechanisms inside organic superstructures.

Nucleation and Organic Superstructures. Before decomposition, the solution is composed of several species arising from the reaction of the highly reactive $\{Fe[N(SiMe_3)_2]_2\}_2$ with PA, HDA, or both. Since the reaction is carried out with less than

(16) Chen, M.; Pica, T.; Jiang, Y.-B.; Li, P.; Yano, K.; Liu, J. P.; Datye, A. K.; Fan, H. *J. Am. Chem. Soc.* **2007**, *129*, 6348–6349.

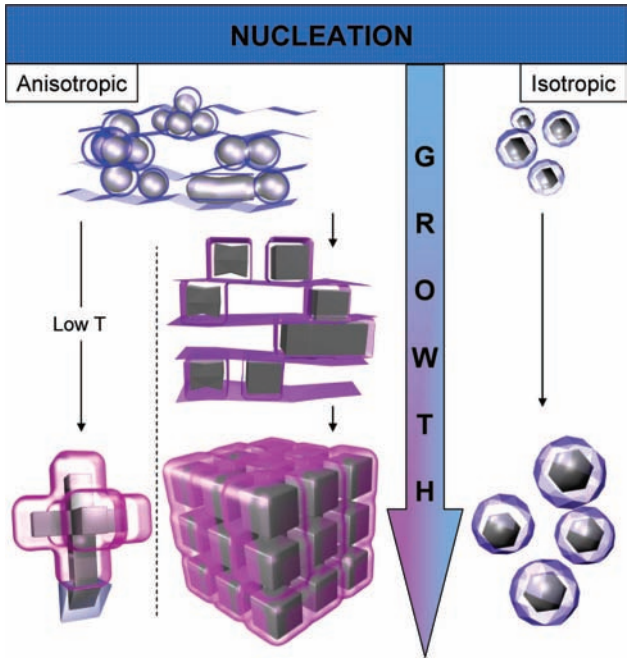

Figure 8. Schematic view of the two environment-dependent growth routes (nucleation in two different environments). The blue color indicates an amine-rich environment, and the violet color is used to represent an organic shell composition that preferentially stabilizes the {100} facets of the iron NPs.

2 equiv of PA, we cannot expect that the iron precursor transforms selectively into one species, such as bis(carboxylate)iron(II). This means that the kinetics of the decomposition is likely governed by at least two reactions: the fast decomposition of presumably an amido iron(II) complex/cluster, which feeds the nucleation step, and the slow decomposition of presumably a carboxylate iron(II) complex, which feeds the growth step, in agreement with the difference in stability of amido and carboxylate Fe(II) derivatives. This hypothesis is confirmed by the Mössbauer study: there is still a small contribution of iron(II) complexes after 48 h. Thus, we can consider that nucleation and growth are strictly separated in this reaction as a result of the difference in stability of the two iron sources, at any decomposition temperature from 100 to 150 °C.

Besides acting as stabilizing agents, the PA/HDA surfactant pair has the ability to self-organize into long-range lamellar structures or bilayers. As far as we know, the phase diagram for such a system in an apolar solvent has never been reported in the literature. However, such a phase has previously been observed in water for a surfactant mixture of the same kind.[14] Lamellar self-organization in water, which is typical of salt-free catanionic systems, has been deeply investigated by Zemb et al.[14] They evidenced the formation of stable micrometric objects made up of surfactant bilayers; the objects' shape and stability were dependent upon the acid/amine ratio. By means of calculations, these authors also showed that the bilayers preferentially adopt a close-packed conformation when the acid/amine ratio is 1:2. These observations can also be applied to the acid-concentration dependence in our system, especially in the concentration range of interest where we detect superstructures. A similar oleic acid/oleylamine mixture was shown by Chen et al.[16] to drive the formation of FePt nanorods through the formation of a hexagonal reverse-liquid-crystal mesophase in the organic reaction solution. They assumed that water traces produced by acid−amine condensation were playing a major role in the stabilization of such a mesophase.[17] This last point highlights the importance of knowing and understanding exactly what composes and strengthens such an organized system. In our case, we have not investigated the presence of water, since we think it would react with the excess hexamethyldisilazane coming from the iron dimer decomposition. We are currently working on the possible role of these light silicon derivatives. However, the organic superstructures' contrast seen in the TEM images suggests an iron upload. Carboxylate iron(II) species here could play the role of a structuring agent. Previous results show that it is possible to take advantage of such a coordination system to grow stable 1D iron(II) structures held together by dicarboxylate ligands.[18] The PA/HDA lamellar phase together with this structuring agent dictate the formation of the iron(II) reservoir and ensure its stability, as shown by the Mössbauer spectra. Evidence that such organic superstructures guide the growth of NPs has been reported very recently in regard to the synthesis of ultrathin Au nanowires.[19] Yang and co-workers[19a] and Xia and co-workers[19b] have explained that an Au^{+}−oleylamine complex self-assembles into mesostructures that serve as a template for the anisotropic growth. In our case, after a fast nucleation step, the growth would then take place in an inhomogeneous solution in which two systems have to be considered: the one "inside" the organic superstructures (i.e., in an anisotropic medium) and the one "outside" them (i.e., in an isotropic medium). The iron(II) reservoir would then influence both the kinetics of the growth and its environment.

Growth inside Organic Superstructures. The growth mechanism is a complex combination of simultaneous reactions, but we have identified two main successive parts: (a) the coalescence of nuclei when the medium is amine-rich and (b) the growth of the {100} iron facets when the medium becomes acid-rich. In part (a), the ligand shell around the NPs is amine-rich, since most of the acid is stored inside the iron(II) reservoir. These conditions favor the coalescence of nanoparticles, as observed during the initial 6 h of reaction. Coalescence in an amine-rich medium was previously reported in the case of Pt NPs: wormlike NPs stabilized by HDA were formed.[20] In the present case, the decomposition of $\{Fe[N(SiMe_3)_2]_2\}_2$ in the presence of HDA alone also yields wormlike iron NPs because of the relatively low binding energy of HDA (see Figure 6a). Therefore, the reaction would produce anisotropic NPs at first, as a result of coalescence in the anisotropic environment provided by the organic superstructures (see the schematic drawing in Figure 8). Some of these NPs display one dimension larger than the size of the final NPs (48 h). The transition between the two growth regimes seems to be effective when the acid concentration around the growing NPs is high enough to significantly stabilize the {100} iron facets. After 12 h of reaction, about half of the acid has been released, since about half of the iron(II) reservoir has been consumed, as shown by the Mössbauer spectra and confirmed by the SQuID measurements. This corroborates the increased number of well-defined facets observed on the TEM pictures (see Figure 2d). The lamellar structure of the ligand self-organization reinforces this effect by preferentially stabilizing the parallel {100} facets. The presence of organic superstructures in this system is therefore

(17) Wu, H.; Yang, Y.; Cao, Y. C. *J. Am. Chem. Soc.* **2006**, *128*, 16522–16523.
(18) Sanselme, M.; Grenèche, J. M.; Riou-Cavellec, M.; Férey, G. *Chem. Commun.* **2002**, 2172–2173.
(19) (a) Huo, Z.; Tsung, C.; Zhang, X.; Yang, P. *Nano Lett.* **2008**, *8*, 2041–2044. (b) Lu, X.; Yavuz, M. S.; Tuan, H.-Y.; Korgel, B. A.; Xia, Y. *J. Am. Chem. Soc.* **2008**, *130*, 8900–8901.

the key point for ensuring the formation of monocrystalline cubic NPs of bcc iron. At the transition between part (a) of the reaction and part (b), we can observe both the formation of cubic nanoparticles resulting from the filling of octapods and the corrosion of large anisotropic particles into cubes. This is in agreement with the concomitant action of oriented growth and repair steps. The first of these processes is evidenced by the presence of monocrystalline filled octapods after 25 h of reaction (see Figures 2e and 3a and Figure S2e in the Supporting Information). Similar objects have been observed in the Pt system studied by Tilley et al.[21] Their presence was assigned to a change in the growth regime from the kinetically controlled growth of the Pt {111} planes to the growth of the more stable {100} planes through a diffusion regime of the adatoms. This change was correlated with a decrease in the Pt atom concentration during the reaction. At the end of the reaction, these particles were then assumed to be nanocubes on their way to completion. This is in quite good agreement with our observations for this Fe system, especially because of the slow consumption of the iron(II) reservoir and the transition from an amine-rich to an acid-rich growth environment. Since we only get nanocubes at the end of the reaction, we can assume that the growth at this stage is governed by the minimization of the total energy of the nanoparticle/ligand system. Since the particles grow in a mesophase that tends to form a stable long-range lamellar structure because of the nature of the aliphatic long-chain ligands, the best energetic compromise is indeed given by the formation of bcc iron particles exposing parallel {100} facets. Moreover, for the same volume, a cubic shape would be preferred over an anisotropic plane-parallel one in order to keep the surface/volume ratio minimal. This means that ripening necessarily occurs to preserve the cubic shape of the growing NPs, which was not obvious a priori in such an anisotropic environment. A digestive ripening process, i.e., the repair step, is evidenced by the corrosion of the large anisotropic NPs, which are not detected anymore at the end of the reaction (see Figures 2f and 3b).

The previous section has emphasized the importance of the variation of the acid/amine ratio during the growth and ripening reactions. However, this ratio can vary even as a function of the organic-shell curvature in the anisotropic reaction medium. Thus, it has been reported by Zemb et al.[13] that the acid/amine ratio inside micrometric objects composed of surfactant bilayers varies as a function of the position in the object (facets, edges, or corners). This difference of acid/amine ratios is governed by the curvature of the objects, the planes/facets being the reference. According to this, we suggest that the curvature around the {110} and {111} facets could be responsible for local fluctuations in the acid concentration. Thus, the ligand shell would present an excess of amine around the edges and the corners of the nanocubes, causing curvature of one sign, but present an excess of acid around two {100} facets, forming an opposite curvature (see Figure 9). Finally, excess amine would favor local growth while excess acid would favor local corrosion, the reference composition being the one stabilizing the {100} facets. These proposed ripening and repair mechanisms are both responsible for the formation of cubic nanoparticles.

Growth outside the Organic Superstructures. Outside the organic superstructures, the growth is isotropic. According to the assumption that the organic superstructures must be composed of most of the acid initially introduced into the solution (which was confirmed by the acid-concentration influence; see the Results and also below), we presume that the medium

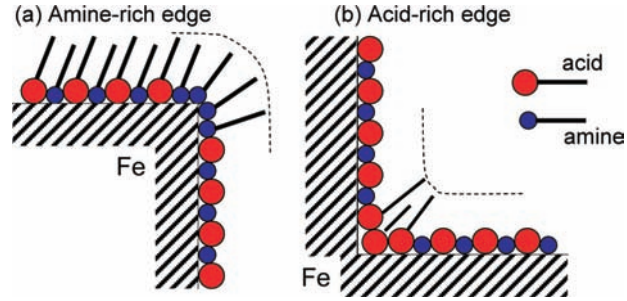

Figure 9. Schematic view of the ligand-shell organization along the facets and two kinds of edges of the NPs.

outside these organizations is amine-rich, in agreement with the isotropic shape of the NPs observed in this medium. However, one has to notice that the spherical NPs are polycrystalline (see Figure S5 in the Supporting Information), likely with preferential exposure of only the {100} facets to the solution, which still contains some acid. Finally, there is no further stabilization of only parallel facets, since there is no organic superstructure around.

In summary, the local acid concentration is the key factor that orientates the growth of the nanoparticles, whether we consider it inside or outside the organic superstructures. Thus, since the long-chain acid is incorporated by complexation in the iron(II) reservoir and participates in the organic superstructure, any concentration change has a drastic effect on the environment-dependent growth. At low concentrations of PA (between 1.0 and 1.3 equiv), the stabilization of long-range ligand self-organization is not favored. The nucleation and growth occur in an isotropic environment, yielding small, spherical NPs. These NPs are polycrystalline and expose at their surface {100} facets stabilized by the introduced acid. The narrow size dispersion suggests that nucleation and growth are strictly separated, as we supposed previously. At PA concentrations equal to or higher than 1.4 equiv, a long-range organic lamellar phase, i.e., a significant iron(II) reservoir, is formed. An increase of the PA concentration clearly slows down some of the reaction kinetics (reservoir decomposition, oriented growth, repair mechanism) because of the molecular species stabilization. In addition, the acid concentration changes from the beginning to the end of the reaction because of the slow consumption of the iron(II) reservoir. As the acid rules the stability of the NP surface, this change in concentration modulates the growth of the NPs, which proceeds first by coalescence and then by oriented growth, ripening, and the repair mechanism inside the ligand self-organization.

The influence of the temperature correlates well with the proposed model. As a matter of fact, the ripening and repair processes in particular are slowed when the reaction is performed at lower temperature. After 7 days at 135 °C, the NPs are large (~46 nm) and clearly result from coalescence of smaller ones. They seem to be on their way to completion to become cubic. Because the consumption of the iron(II) reservoir has been slowed, the growth environment remains amine-rich for a long time, and the coalescence is therefore prolonged. The result is a decrease in the number of nuclei, leading then to few but large NPs after 7 days. The SQuID and Mössbauer experiments confirm the reaction is, after 7 days, at a similar stage as the reaction performed at 150 °C after 6 h and 12 h (see Figures S15−S16 and Table S2 in the Supporting Information). After 21 days at 120 °C, we obtain monocrystalline stars that expose {100} facets, as revealed by HRTEM pictures (see Figure

5b−d). The transition from isotropic particles to stars has previously been reported for several systems, such as Rh,[22] CdS,[23] PbS, and Pt systems.[24,25] Interpretations of these temperature-dependent or reduction-kinetics-dependent growths usually invoke a seeded-growth mechanism[24] or a delicate balance between kinetic and thermodynamic regimes.[21] In our case, at 120 °C, nucleation is very slow, growth proceeds through coalescence and preferential {100} facet growth, and the repair mechanism is also presumably very slow. The result is seeded growth, i.e., an oriented growth along the initial directions given by the nuclei, leading to the observed stars for which no effective repair mechanism is available.

Conclusion

In this paper, we have reported a complete study aimed at understanding the growth of iron NPs by an organometallic route. The effect of several key parameters, including the reaction time, the temperature, and the surfactant concentrations, has been investigated, leading to the development of a model involving an environment-dependent growth mechanism. The presence of organic superstructures filled with iron(II) species at the very beginning of the reaction is a key point in understanding the shape control of the final product. Indeed, the nucleation and growth can occur either outside these templates (i.e., in an isotropic environment) or inside them (i.e., in an anisotropic environment). In the first case, we obtain spherical polycrystalline NPs having mean sizes that increase with the carboxylic acid concentration, as expected. In the second case, the reaction monitoring reveals several steps: (i) nucleation, (ii) coalescence favored by an amine-rich environment, and (iii) growth and repair mechanisms in an acid-rich environment. These three main steps lead to cubic NPs organized into superstructures: the nanocube superlattices. The evolution of the environment from amine-rich to acid-rich is directly correlated with the decomposition of the iron(II) reservoir, which releases carboxylic acid into the medium. Iron nanocubes are formed inside these templates and then directly assembled into close-packed micrometric superlattices. The growth of anisotropic objects such as stars is obtained by decreasing the reaction temperature, which modifies the relative kinetics of the nucleation, growth, and repair steps. As a whole, this study sheds light on a versatile, complex system, allowing control of the formation of cubic (side length from 13 to 27 nm) and spherical (diameter from 1.5 to 9.4 nm) iron nanoparticles.

Acknowledgment. L.-M.L. thanks the French Ministry of National Education and Research for her MENRT grant. We thank A. Mari and J.-F. Meunier for help with the SQuID and Mössbauer measurements and V. Collière for SEM characterization. We also thank K. Soulantica and F. Dumestre for fruitful discussions.

Supporting Information Available: Figures S1−S17 and Tables S1 and S2. This material is available free of charge via the Internet at http://pubs.acs.org.

JA805719C

(20) Ramirez, E.; Erades, L.; Philippot, K.; Lecante, P.; Chaudret, B. *Adv. Funct. Mater.* **2007**, *17*, 2219–2228.
(21) Ren, J.; Tilley, R. D. *J. Am. Chem. Soc.* **2007**, *129*, 3287–3291.
(22) Hoefelmeyer, J. D.; Niesz, K.; Somorjai, G. A.; Tilley, T. D. *Nano Lett.* **2005**, *5*, 435–438.
(23) Lee, S.-M.; Cho, S.-N.; Cheon, J. *Adv. Mater.* **2003**, *15*, 441–444.
(24) Lee, S.-M.; Jun, Y.-W.; Cho, S.-N.; Cheon, J. *J. Am. Chem. Soc.* **2002**, *124*, 11244–11245.
(25) Chen, J.; Herricks, T.; Xia, Y. *Angew. Chem., Int. Ed.* **2005**, *44*, 2589–2592.